α-Tubulin K40 acetylation is required for contact inhibition of proliferation and cell–substrate adhesion

Andrea Aguilar[a], Lars Becker[b], Thomas Tedeschi[c], Stefan Heller[b], Carlo Iomini[c], and Maxence V. Nachury[a]

[a]Department of Molecular and Cellular Physiology and [b]Department of Otolaryngology–Head and Neck Surgery, Stanford University School of Medicine, Stanford, CA 94305; [c]Departments of Ophthalmology and of Developmental and Regenerative Biology, Friedman Brain Institute, Mount Sinai School of Medicine, New York, NY 10029

ABSTRACT **Acetylation of α-tubulin on lysine 40 marks long-lived microtubules in structures such as axons and cilia, and yet the physiological role of α-tubulin K40 acetylation is elusive. Although genetic ablation of the α-tubulin K40 acetyltransferase αTat1 in mice did not lead to detectable phenotypes in the developing animals, contact inhibition of proliferation and cell–substrate adhesion were significantly compromised in cultured *αTat1*$^{-/-}$ fibroblasts. First, *αTat1*$^{-/-}$ fibroblasts kept proliferating beyond the confluent monolayer stage. Congruently, *αTat1*$^{-/-}$ cells failed to activate Hippo signaling in response to increased cell density, and the microtubule association of the Hippo regulator Merlin was disrupted. Second, *αTat1*$^{-/-}$ cells contained very few focal adhesions, and their ability to adhere to growth surfaces was greatly impaired. Whereas the catalytic activity of αTAT1 was dispensable for monolayer formation, it was necessary for cell adhesion and restrained cell proliferation and activation of the Hippo pathway at elevated cell density. Because α-tubulin K40 acetylation is largely eliminated by deletion of αTAT1, we propose that acetylated microtubules regulate contact inhibition of proliferation through the Hippo pathway.**

Monitoring Editor
Erika Holzbaur
University of Pennsylvania

Received: Nov 14, 2013
Revised: Apr 8, 2014
Accepted: Apr 9, 2014

INTRODUCTION

A variety of posttranslational modifications (PTMs) decorate α- and β-tubulin. Although some PTMs have been involved in the regulation of microtubule dynamics and the accessibility to microtubule-associated proteins or severing enzymes (Janke and Bulinski, 2011), the precise function of most PTMs is largely elusive. Acetylation on lysine 40 of α-tubulin marks long-lived microtubules found in mitotic spindles, axons, and cilia and is generally believed to be a consequence rather than a cause of microtubule stabilization (Rosenbaum, 2000; Palazzo *et al.*, 2003). However, the physiological role of αK40 acetylated microtubules is unclear. Until recently, acetylated tubulin levels could only be manipulated by interfering with the function of the K40 deacetylases HDAC6 and SIRT2 (Hubbert *et al.*, 2002; North *et al.*, 2003). Problematically, these enzymes have multiple substrates and deacetylase-independent functions (Zhang *et al.*, 2007; Zilberman *et al.*, 2009). The recent discovery of αTat1, the major α-tubulin K40 acetyltransferase in *Tetrahymena*, nematodes, and cultured mammalian cells (Akella *et al.*, 2010; Shida *et al.*, 2010), offers a unique opportunity to shed light on the physiological importance of tubulin acetylation. In particular, genetic ablation of the *αTat1* orthologue *mec-17* in nematodes revealed that acetylation of α-tubulin on lysine 40 is essential for touch sensation and integrity of the axonal microtubules in touch receptor neurons (Akella *et al.*, 2010; Shida *et al.*, 2010; Cueva *et al.*, 2012; Topalidou *et al.*, 2012). However, a general and conserved function for α-tubulin K40 acetylation remains to be determined.

Although no overt phenotype was observed in *αTat1*$^{-/-}$ mice, studies of cultured mouse fibroblasts revealed a role for α-tubulin K40 acetylation in cell adhesion and contact inhibition of proliferation. Our functional results suggest that acetylated microtubules promote Hippo signaling by facilitating Merlin delivery to its substrates.

This article was published online ahead of print in MBoC in Press (http://www.molbiolcell.org/cgi/doi/10.1091/mbc.E13-10-0609) on April 17, 2014.

Address correspondence to: Maxence Nachury (nachury@stanford.edu).

Abbreviations used: FA, focal adhesion; PTM, posttranslational modification.

RESULTS

αTat1 is the major tubulin acetyltransferase in vivo

To assess the contribution of αTat1 to α-tubulin K40 acetylation in vivo and evaluate the functional significance of this modification, we generated a mouse lacking most of the coding exons of *αTat1* using ES cells from the National Institutes of Health Knock-Out Mouse Project (KOMP; Supplemental Figure S1A). The genomic ablation of *αTat1* was confirmed by PCR of genomic DNA (Supplemental Figure S1A), and the absence of Tat1 protein was confirmed by immunoblotting of brain extracts (Figure 1A). Brain extracts were chosen because α-tubulin K40 acetylation is highest in brain compared with other organs (Zhang *et al.*, 2008). Whereas multiple isoforms of αTat1 ranging between 35 and 40 kDa (as well as possible degradation products) were detected throughout neural development and in the adult brain of wild-type animals, no αTat1 protein was detected in the *αTat1*$^{-/-}$ mice (Figure 1A). Concordantly, K40 acetylated α-tubulin was undetectable either by immunoblotting of brain lysates (Figure 1A) or immunohistochemistry on adult brain sections (Supplemental Figure S1B).

Besides αTat1, several enzymes have been proposed to bear α-tubulin acetyltransferase activity, including the histone acetyltransferase Elp3 (Solinger *et al.*, 2010). Because the evidence for Elp3 being an α-tubulin K40 acetyltransferase is controversial (Creppe *et al.*, 2009; Shida *et al.*, 2010; Solinger *et al.*, 2010; Cheishvili *et al.*, 2011; Miskiewicz *et al.*, 2011), we sought to assess directly the ability of Elp3 to acetylate microtubules in immortalized *αTat1*$^{-/-}$ mouse embryonic fibroblasts (MEFs), which are devoid of acetylated microtubules (Supplemental Figure S1C; Friedmann *et al.*, 2012). Although transient transfection of green fluorescent protein (GFP)–αTat1 successfully restored microtubule acetylation, no K40 acetylated α-tubulin was detected in cells transfected with GFP-ELP3, even at the highest levels of ELP3 expression (Figure 1B). Thus, as previously observed in Ptk2 cells (Shida *et al.*, 2010), Elp3 does not harbor any intrinsic α-tubulin K40 acetyltransferase activity. Although no acetylated microtubules were found in interphase *αTat1*$^{-/-}$ MEFs, we consistently detected very low levels of K40 acetylated α-tubulin at the spindle of mitotic *αTat1*$^{-/-}$ cells (Figure 1C), suggesting that a second, and very minor, α-tubulin K40 acetyltransferase activity might exist in mice. Taken together, our results show that αTat1 is the main tubulin acetyltransferase in mouse brain and cultured fibroblasts.

αTat1 is dispensable for mammalian brain development

Although the deletion of *αTat1* resulted in mice devoid of K40 acetylated α-tubulin, these animals are viable and do not exhibit any overt phenotype (Supplemental Figure S1D), in agreement with recent reports (Kalebic *et al.*, 2013b; Kim *et al.*, 2013). α-Tubulin K40 acetylation reaches the highest levels in the brain, where nearly 30% of α-tubulin is acetylated at K40 (D. Portran and M. V. Nachury, unpublished data). Yet, aside from a recently described enlargement of the dorsal part of the granular layer of the dentate gyrus (Kim *et al.*, 2013), no major defect in the global brain architecture was evident in adult *αTat1*$^{-/-}$ brain sections (Supplemental Figure S1E).

Aside from the brain, other organs are characterized by notable arrays of acetylated microtubules, such as the maturing corneal endothelium and its perinuclear basket of acetylated and detyrosinated microtubules (Blitzer *et al.*, 2011) and the pillar cells of the inner ear, which offer mechanical support to the sensory hair cells (Tannenbaum and Slepecky, 1997; Szarama *et al.*, 2012). Loss of αTat1 did not alter the perinuclear array of detyrosinated microtubules in the corneal endothelium (Supplemental Figure S2A). Further, assessment of auditory function revealed intact hearing ability in *αTat1*$^{-/-}$ mice (Supplemental Figure S2B), despite the importance of acetylated microtubules for mechanosensation in nematodes. Thus the inner ear, cornea, and brain—all of them tissues with high levels of acetylated microtubules—appear unaffected by αTat1 loss.

One possible explanation for the apparent lack of neural phenotype in *αTat1*$^{-/-}$ mice is functional compensation by other tubulin PTMs. To address this possibility, we measured the levels of tubulin PTMs associated with microtubule stabilization in wild-type and *αTat1*$^{-/-}$ brain lysates using quantitative immunoblotting and found no major differences (Figure 1D). We also assessed the organization of long-lived (detyrosinated) and dynamic (tyrosinated) microtubules in the cerebellar molecular layer and the hippocampus. In these regions, the spatial distribution of detyrosinated and tyrosinated tubulin was unchanged in *αTat1*$^{-/-}$ mice compared with wild-type mice (Supplemental Figure S3A). In particular, the global cytoarchitecture of the Bergmann glia (glial fibrillary acidic protein [GFAP] and S100β positive), a structure rich in tyrosinated and detyrosinated tubulin, was unaltered in *αTat1*$^{-/-}$ mice (Supplemental Figure S3A).

The Purkinje cells of the cerebellar cortex express high levels of αTat1 (Kalebic *et al.*, 2013a), and it was proposed that α-tubulin K40 acetylation promotes dendritogenesis in Purkinje cells (Ohkawa *et al.*, 2007, 2008). However, polyglutamylated tubulin staining of Purkinje cells revealed that their dendritic arborization is unaffected by removal of αTat1 (Supplemental Figure S3B).

In mature neurons, acetylated microtubules are highly enriched in axons compared with dendrites, and there is conflicting evidence for acetylated microtubules playing a role in axonal specification and neuronal polarization (Witte *et al.*, 2008; Li *et al.*, 2012). To resolve this controversy, we assessed axonal morphology by polyglutamylated tubulin immunostaining of brain cryosections. We found that the morphology of axonal tracts and single axons was similar in wild-type and *αTat1*-deficient mice (Supplemental Figure S3B).

Finally, because K40 acetylated α-tubulin is highly enriched in cilia and αTat1 is universally conserved in ciliated organisms and accelerates ciliogenesis in cultured mammalian cells (Shida *et al.*, 2010), we analyzed ciliogenesis in wild-type and *αTat1*$^{-/-}$ animals. In agreement with recent reports (e.g., Kalebic *et al.*, 2013b), no major differences in motile or primary cilia (ependymal cells and corneal endothelial cells, respectively) were observed in the absence of αTat1 (Figure 1E).

Thus the global cerebral and cellular architecture is preserved in the absence of αTat1, indicating that α-tubulin K40 acetylation is dispensable for brain development and neuronal polarization.

αTat1 is required for contact inhibition of proliferation

Controlled cell proliferation is a complex and highly regulated process central to morphogenesis, organ size control, and wound healing (McClatchey and Yap, 2012). In nontransformed cells, proliferation is repressed by cell–cell contacts, leading to cells exiting the cell cycle and organizing into a monolayer upon reaching confluency (Abercrombie, 1962). Loss of contact inhibition is observed in the majority of cancer cell lines and constitutes a hallmark of malignant transformation (Abercrombie, 1979; Hanahan and Weinberg, 2000; Zeng and Hong, 2008). MEFs exhibit robust contact-dependent growth inhibition, forming a polarized quiescent monolayer after 2–3 d of culture (Todaro and Green, 1963; Figure 2A). In contrast, *αTat1*-deficient MEFs cultured for the same amount of time grew into multiple unpolarized cell layers (Figure 2A) with greatly elevated cell density. To quantify cell proliferation and contact inhibition, we seeded wild-type and *αTat1*$^{-/-}$ cells at the same initial density (25% confluency; Supplemental Figure S4A) and allowed them to grow in

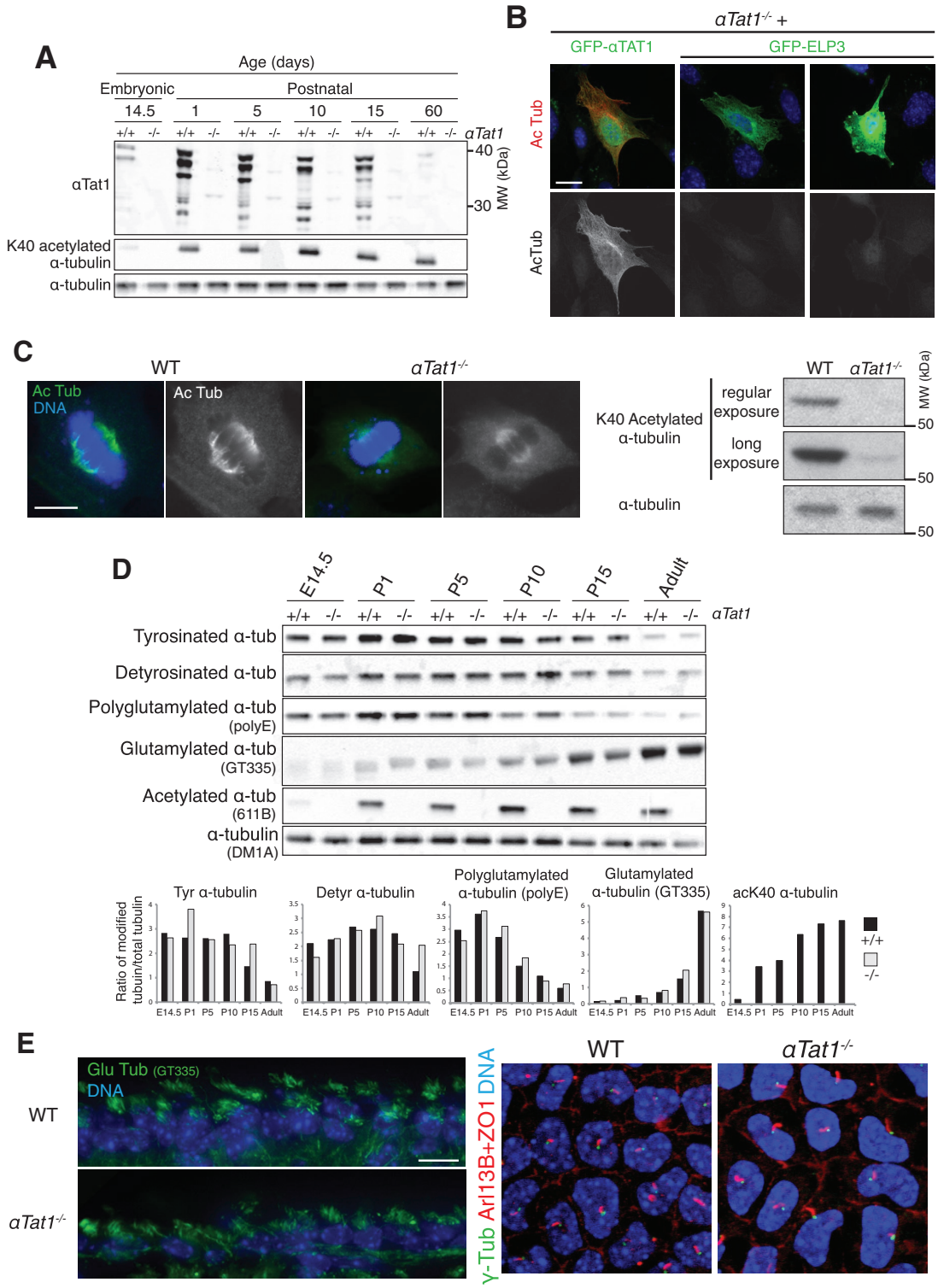

FIGURE 1: αTat1 is the major α-tubulin K40 acetyltransferase in vivo and is dispensable for mammalian CNS development and ciliogenesis. (A) Brain lysates from various developmental stages (E14.5, embryonic day 14.5; P1–P15, postnatal days 1–15) were immunoblotted for the indicated proteins. (B) *αTat1*$^{-/-}$ MEFs were transfected with GFP-αTat1 or GFP-ELP3 (green) and immunostained for GFP (green) and K40 acetylated α-tubulin (red). (C) Left, K40 acetylated α-tubulin immunostaining (green) of *αTat1*$^{+/+}$ and *αTat1*$^{-/-}$ MEFs. Right, *αTat1*$^{+/+}$ and *αTat1*$^{-/-}$ MEFs lysates were immunoblotted for K40 acetylated and total α-tubulin. (D) Brain lysates from *αTat1*$^{+/+}$ and *αTat1*$^{-/-}$ mice at various developmental stages were immunoblotted for various α-tubulin posttranslational modifications. The quantitation of the immunoblots showed no major differences between wild-type and knockout mice. (E) Left, adult brain cryosections were stained with polyglutamylated α-tubulin (GT335 antibody, ependymal motile cilia, green). Right, basal bodies (γ-tubulin, green), primary cilia (Arl13B, red) and the cell–cell junction (ZO-1, red) were labeled in P6 corneal endothelium whole mounts. No defects in motile or primary cilia presence were noted in *αTat1*$^{-/-}$ mice. Scale bars: B, 20 μm; C, 10 μm; E, 10 μm.

the presence of frequently replenished serum. Two days after seeding, wild-type cells reached a stereotypical saturating density (Todaro *et al.*, 1965) and stayed quiescent for an extended period of time (Figure 2B). Strikingly, *αTat1*$^{-/-}$ cells grew considerably faster, bypassing the saturating density of wild-type cells soon after day 1. Furthermore, the saturating density of *αTat1*$^{-/-}$ cells was more than fourfold higher than that seen for control cells (Figure 2B) and may represent an underestimate, given the detachment of loosely adherent *αTat1*$^{-/-}$ cells during the washes preceding cell counting. To verify that the observed effects resulted from the loss of *αTat1*, we generated cell lines stably expressing GFP, GFP-αTAT1, or the acetyltransferase-dead GFP-αTAT1[D157N]. Whereas GFP-αTAT1 expression restored tubulin acetylation to wild-type levels, expression of GFP or GFP-αTAT1[D157N] at the same levels as GFP-αTAT1 did not alter tubulin acetylation (Figure 2, C and D, and Supplemental Figure S4B). Of importance, stable expression of GFP-αTAT1, but not GFP alone, was able to restore the saturating density to near-wild-type levels (Figure 2B). Similarly, restoration of monolayer formation was seen upon reintroduction of wild-type GFP-αTAT1, but no rescue was observed for GFP alone (Figure 2A).

Unexpectedly, recent studies suggested that αTat1 possesses a nonenzymatic function in nematodes (Topalidou *et al.*, 2012). Similar to GFP alone, GFP-αTAT1[D157N] was unable to restore the saturating density of *αTat1*$^{-/-}$ MEFs to near-wild-type levels or the polarity of the monolayer (Figure 2B). Surprisingly, the catalytically dead form of αTat1 rescued monolayer formation (Figure 2A), suggesting that tubulin acetylation is dispensable for the regulation of monolayer formation. Consistent with the greater number of cells contained within the monolayer, cell size was reduced at confluency in *αTat1*$^{-/-}$ cells expressing GFP-αTAT1[D157N] (Figure 2A and Supplemental Figure S4D). Thus our results indicate that the acetyltransferase activity of αTat1 is not required for monolayer formation but may be necessary for regulating cell size—and thus number—at confluency. Alternatively, it is conceivable that the D157N mutant of TAT1 retains catalytic activity against another substrate than tubulin and acetylation of this alternative substrate prevents growth beyond the monolayer stage.

Studies over the past decade have revealed a critical role for the Hippo tumor-suppressor pathway in contact inhibition of proliferation. At low cell density, the Yes-associated protein (YAP) and its partner, TAZ, accumulate in the nucleus to activate the transcription of target genes that promote cell proliferation. When cell density increases, Hippo signaling triggers a kinase cascade that culminates in the nuclear exclusion of YAP through direct phosphorylation (Zhao *et al.*, 2011). Cell–cell contacts and the actin cytoskeleton are well-characterized players in Hippo signaling. In addition, microtubule integrity is required for proper Hippo signaling (Zhao *et al.*, 2012), but the specific role of acetylated microtubules in this process remains untested. To assess whether the loss of contact inhibition observed in the absence of αTat1 could be due to defective Hippo signaling, we monitored YAP/TAZ activity using the transcriptional reporter 8xGTIIC-luc (Dupont *et al.*, 2011). As previously reported, YAP/TAZ activity was high in sparse cells and diminished by more than fourfold as cells reached confluency (Figure 3, A and B). In contrast, *αTat1*$^{-/-}$ MEFs exhibited elevated YAP/TAZ activity at low cell density and failed to repress the YAP/TAZ activity in response to increasing cell density (Figure 3, A and B). As a result, *αTat1*$^{-/-}$ MEFs required cell densities nearly 10 times higher than wild-type MEFs to achieve the same levels of YAP/TAZ activity (Figure 3A). This suggests that the expression of proliferation-promoting genes is constitutively high in cultured *αTat1*$^{-/-}$ cells and that in the absence of αTat1, MEFs are largely insensitive to cell density cues. Of interest, stable expression of GFP-αTAT1 in *αTat1*$^{-/-}$ cells restored density-dependent down-regulation of YAP/TAZ activity, even though it was unable to rescue the high levels of YAP/TAZ activity in sparse cells (Figure 3, C and D). It is intriguing that introduction of the acetyltransferase-deficient GFP-αTAT1[D157N] in *αTat1*$^{-/-}$ cells reduced YAP/TAZ activity in sparse cells but failed to restore the sensitivity to cell density (Figure 4, C and D). This could indicate that the ratio of YAP/TAZ activity between sparse and dense conditions, rather than the absolute activity of YAP/TAZ, controls cell number at confluency.

Merlin/NF2, an upstream component of the Hippo signaling cascade, is so far the sole protein in the Hippo pathway shown to interact with microtubules (Muranen *et al.*, 2007; Bensenor *et al.*, 2010). Most relevant to our study, Merlin is found along acetylated microtubules (Figure 3E; Smole *et al.*, 2014), and the microtubule-dependent transport of Merlin is required for nuclear exclusion of YAP (Bensenor *et al.*, 2010). We therefore hypothesized that acetylated microtubules promote Hippo signaling by facilitating Merlin transport to its substrates. Strikingly, in the absence of αTat1, Merlin was no longer found along microtubules. Instead, Merlin was diffusely distributed in the cytoplasm (Figure 3E and Supplemental Figure S4C), suggesting that acetylated microtubules are required for Merlin transport.

Collectively these experiments reveal a crucial role for αTat1 in contact inhibition. In particular, they show that acetylated microtubules are required for proper Hippo signaling, likely through the control of Merlin localization.

αTat1 is essential for cell adhesion

It is intriguing that *αTat1*$^{-/-}$ MEFs exhibited defective Hippo signaling even at cell densities at which cell–cell contacts are absent (Figure 3A and Supplemental Figure S4C). This result suggested that αTat1 might also influence Hippo signaling through a different pathway than contact inhibition. Given that the Hippo pathway and cell–substrate adhesion are closely linked (Katagiri *et al.*, 2006; Artemenko *et al.*, 2012) and that HDAC6-knockout MEFs are hyperadhesive to substrate (Tran *et al.*, 2007), we investigated cell adhesion in *αTat1*$^{-/-}$ cells. During routine handling of *αTat1*$^{-/-}$ MEF cultures, we noticed that cells detached easily upon medium change. Furthermore, *αTat1*$^{-/-}$ MEFs exhibited reduced spreading on the surface of the culture dish (Figure 4A), and *αTat1*$^{-/-}$ MEFs were more sensitive to trypsin exposure than wild-type cells (Figure 4B). Together these observations suggested that cell–substrate adhesion is impaired in the absence of αTat1. Because focal adhesions (FAs) are the structures responsible for cellular attachment to the growth substrate, we asked whether they are altered in *αTat1*$^{-/-}$ cells. Staining for vinculin, a central component of focal adhesions, revealed that in *αTat1*$^{-/-}$ cells, the number of FAs is significantly reduced and their size is diminished (Figure 4C). We next examined actomyosin stress fibers, which connect and pull onto nascent FAs to promote their growth and maturation. In *αTat1*$^{-/-}$ cells, actin staining revealed a reduced number of stress fibers and a disorganized actin cytoskeleton (Figure 4C*)*. Instead of long stress fibers connecting FAs on opposite sides of the cell, *αTat1*$^{-/-}$ cells contained short stress fibers distributed near the periphery of the cell and oriented tangentially to the edge of the cell. These observations suggested that *αTat1*$^{-/-}$ cells might be unable to mature nascent FAs through tension applied by stress fibers. How could α-tubulin K40 acetylation affect FAs and stress fibers? Over the years, evidence for cross-talk between the microtubule and the actin cytoskeletons has accumulated (Wang *et al.*, 2001; Stehbens and Wittmann, 2012). In particular, microtubule depolymerization

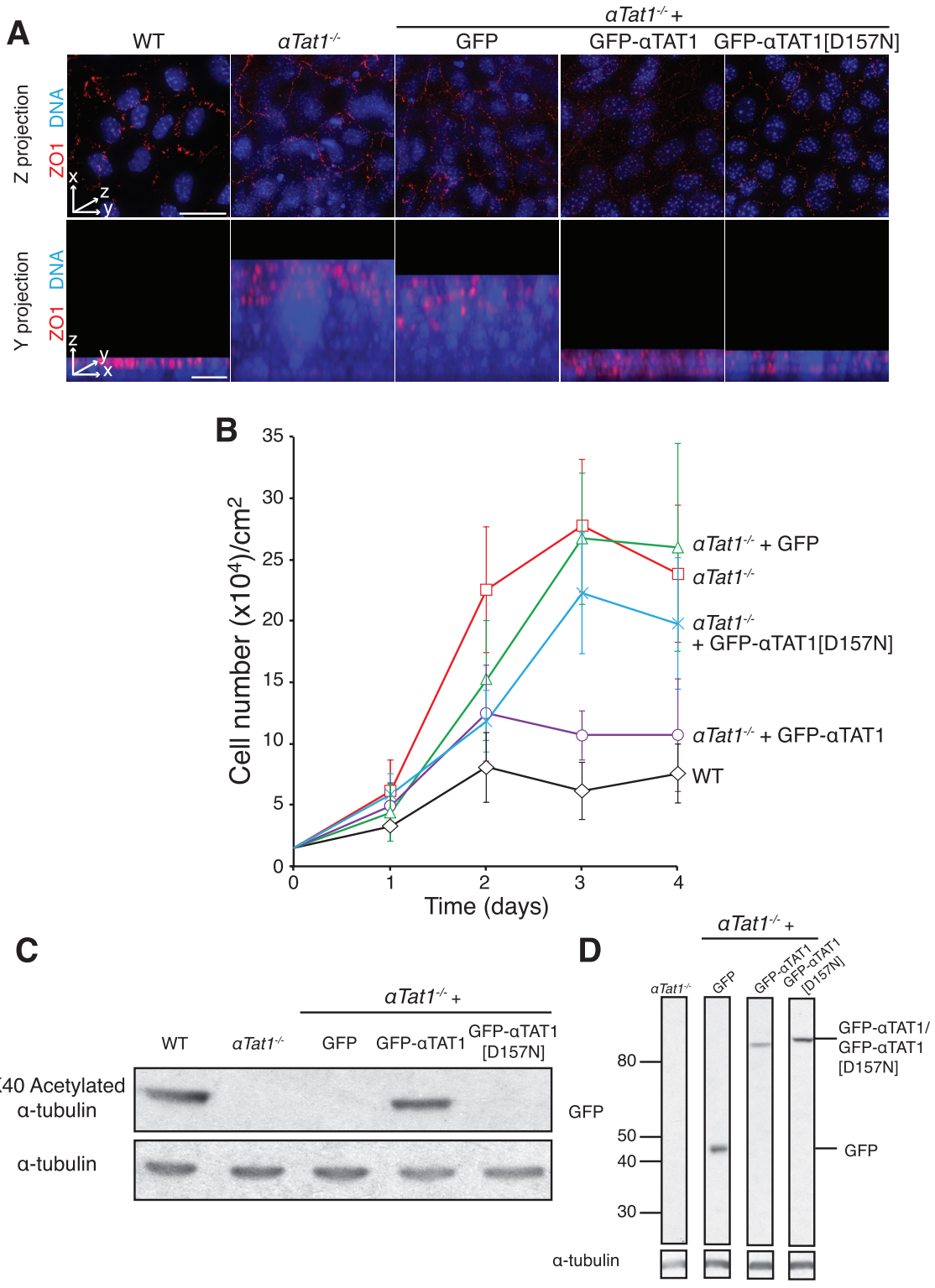

FIGURE 2: αTat1 is required for contact inhibition of proliferation. (A) *αTat1*$^{+/+}$, *αTat1*$^{-/-}$, and *αTat1*$^{-/-}$ cells expressing GFP, GFP-αTAT1, or GFP-αTAT1[D157N] were seeded at 15,000 cells/cm^2. Five days after seeding, cells were fixed and stained for the cell–cell junction marker ZO-1 (red) and DNA (blue). Wild-type cells form a monolayer, seen as clearly separated nuclei in *z*-projection and as a row of evenly distributed nuclei in the projection along the *y*-axis. Expression of GFP-αTAT1 or GFP-αTAT1[D157N] restored monolayer formation, whereas GFP alone did not. In addition, the pattern of ZO1 staining suggests that the bottom layers of the *αTat1*$^{-/-}$ cultures have lost polarity, whereas the top layer does retain some level of polarity. In addition, the rescue of polarity by expression of GFP-αTAT1 appears to only be partial. (B) *αTat1*$^{+/+}$, *αTat1*$^{-/-}$, and *αTat1*$^{-/-}$ cells expressing GFP, GFP-αTAT1, or GFP-αTAT1[D157N] were seeded at 15,000 cells/cm^2, counted every day, and fed every other day. After 2 d of culture, wild-type cells reached a stereotypical saturating density (~60,000 cells/cm^2) and stayed quiescent for the rest of the assay. *αTat1*$^{-/-}$ cells

induces the growth of FAs and stress fibers because of decreased resistance to forces pulling onto FAs in the absence of microtubules (Bershadsky *et al.*, 1996). Whereas numerous massive stress fibers were detected in nocodazole-treated wild-type cells, very few and very thin stress fibers were observed in *αTat1*$^{-/-}$ cells (Figure 4D and Supplemental Figure S5). Consistent with an inability to reinforce FAs upon microtubule depolymerization, *αTat1*$^{-/-}$ cells rapidly rounded up and detached upon nocodazole exposure (Figure 4D and Supplemental Figure S5). Conversely, myosin II inhibition by blebbistatin lowers cortical tension and thereby induces plasma membrane collapse around microtubules to generate microtubule-filled protrusions (Shutova *et al.*, 2008). However, no microtubule-based protrusions were seen in αTat1-deficient cells treated with blebbistatin (Figure 4D and Supplemental Figure S5), suggesting that membrane tension might already be low in untreated *αTat1*$^{-/-}$ cells (likely because of poor substrate adhesion). Collectively these results suggest that αTat1 regulates the size and abundance of FAs and may participate in tension-induced maturation of small, nascent FAs into large, stable FAs.

DISCUSSION

αTat1 is the major tubulin acetyltransferase in mice

αTat1 is the main α-tubulin acetyltransferase for lysine 40 in *Tetrahymena*, *C. elegans*, and mammalian cells (Akella *et al.*, 2010; Shida *et al.*, 2010). In agreement with recent work (Kalebic *et al.*, 2013b; Kim *et al.*, 2013), no acetylated tubulin was detected in the αTat1-deficient mouse brain, either by immunoblot or immunohistochemistry, suggesting that αTat1 is the sole tubulin acetyltransferase in vivo. However, low amounts of acetylated microtubules were detected in mitotic *αTat1*$^{-/-}$ MEFs, indicating the existence of a minor second tubulin acetyltransferase in mammals. This is consistent with the presence of K40 acetylated α-tubulin in stable microtubules of plants such as *Arabidopsis thaliana*, maize, and pine, which bear no αTat1 homologues in their genomes (Gilmer *et al.*, 1999; Huang and Lloyd, 1999; Nakagawa *et al.*, 2013). Given that acetyltransferases with no detectable sequence similarity can share identical substrate specificity (e.g., p/CAF and MOZ are specific histone H3 K14 acetyltransferases that belong to two distinct families of lysine acetyltransferases; Berndsen and Denu, 2008), a search for the second α-tubulin K40 acetyltransferase will need to encompass all putative lysine acetyltransferases.

αTat1 is dispensable for mammalian brain development

Both acetylated α-tubulin and αTat1 have been proposed to participate in major neuronal processes such as neuronal migration, polarization, and function, dendritic growth, and axonal formation (Ohkawa *et al.*, 2008; Witte *et al.*, 2008; Akella *et al.*, 2010; Shida *et al.*, 2010; Li *et al.*, 2012; Topalidou *et al.*, 2012; Kalebic *et al.*, 2013a). Yet, aside from an enlargement of the dorsal part of the dentate gyrus recently described by others (Kim *et al.*, 2013), we did not find any major neural phenotype in *αTat1*-deficient mice. This mirrors published results in which *Hdac6* ablation in mice did not cause significant neural defects (Zhang *et al.*, 2008). More precise examination of the neuroanatomy in *αTat1*$^{-/-}$ mice, and of the enlargement of the granular layer of the dentate gyrus in particular, might reveal subtle anatomical defects and shed light on the subtle functions of acetylated microtubules in the mammalian nervous system.

αTat1 is required for contact inhibition of proliferation

Recently the integrity of the microtubule cytoskeleton was shown to be required for proper contact inhibition of proliferation (Zhao *et al.*, 2012), but the specific role for stable versus dynamic microtubules in this process remains untested. Our results indicate that α-tubulin K40 acetylation is critical for enforcing contact inhibition of proliferation through the Hippo pathway. In particular, we show that tubulin acetylation is required for microtubule association of Merlin, the product of the neurofibromatosis 2 gene. Merlin is found in actin-rich regions and on vesicles transported along microtubules via kinesin-1 and cytoplasmic dynein (Muranen *et al.*, 2007; Bensenor *et al.*, 2010). Given that kinesin-1 and dynein have both been shown to selectively travel along acetylated microtubules in vivo (Dompierre *et al.*, 2007; Cai *et al.*, 2009), we hypothesize that Merlin is transported toward its targets onto acetylated microtubule tracks and that the disappearance of acetylated microtubules leads to decreased Merlin activity in cells. Nonetheless, it is important to note that the role of acetylated microtubules in kinesin-1 motility remains controversial, with a recent in vitro study failing to observe an influence of microtubule acetylation on transport of free kinesin-1 (Walter *et al.*, 2012). It remains possible, however, that tubulin acetylation may influence the movement of motors when they are placed under the typical loads encountered in vivo.

αTat1$^{-/-}$ cells exhibit a striking loss of contact inhibition (Figure 2B). However, the number of *αTat1*$^{-/-}$ cells does appear to plateau after reaching a density fivefold greater than that of wild-type cells. We propose three interpretations for this result. First, at very high density, the cells on the top layer of the *αTat1*$^{-/-}$ multilayered cultures may be too loosely attached and may float away, thus escaping counting. Second (and possibly linked to the first possibility), increased cell death at very high cell density may balance out the increased cell number. Third, *αTat1*$^{-/-}$ cells do down-regulate YAP/TAZ activity at very high density (Figure 3, A and B), which may be sufficient to dampen proliferation.

Stable expression of GFP-αTat1 in *αTat1*$^{-/-}$ cells restored proper cell number and the down-regulation of YAP activity at confluency. However, GFP-αTat1 failed to rescue the high YAP/TAZ activity in sparse *αTat1*$^{-/-}$ cells, as well as the polarity of the monolayer upon confluency. This partial rescue could be explained by the fact that only one out of several isoforms of αTat1 was reintroduced in *αTat1*$^{-/-}$ cells. The introduction of GFP-αTAT1[D157N] in *αTat1*$^{-/-}$ cells rescued monolayer formation and absolute YAP/TAZ activity levels in sparse cells but failed to restore the density-dependent

bypassed the normal saturating density soon after day 1 and reached a saturating density fourfold higher than wild type after 3 d of culture. GFP-αTAT1 expression in *αTat1*$^{-/-}$ cells restored the saturating density to near-wild-type levels, whereas GFP or GFP-αTAT1[D157N] did not. (C) Lysates of *αTat1*$^{+/+}$, *αTat1*$^{-/-}$, and *αTat1*$^{-/-}$ cells expressing GFP, GFP-αTAT1, or GFP-αTAT1[D157N] were immunoblotted for K40 acetylated α-tubulin. Only GFP-αTAT1 expression restores K40 α-tubulin acetylation to wild-type levels. (D) Cell lysates from *αTat1*$^{-/-}$ and *αTat1*$^{-/-}$ cells expressing GFP, GFP-αTAT1, or GFP-αTAT1[D157N] were immunoblotted for GFP and α-tubulin. *αTat1*$^{-/-}$ cell lines expressing GFP and GFP-αTAT1[D157N] were selected to match GFP-αTAT1 expression levels. All lanes come from the same membrane and, as such, have the same exposure. Scale bars: A, 30 μm (top), 5 μm (bottom).

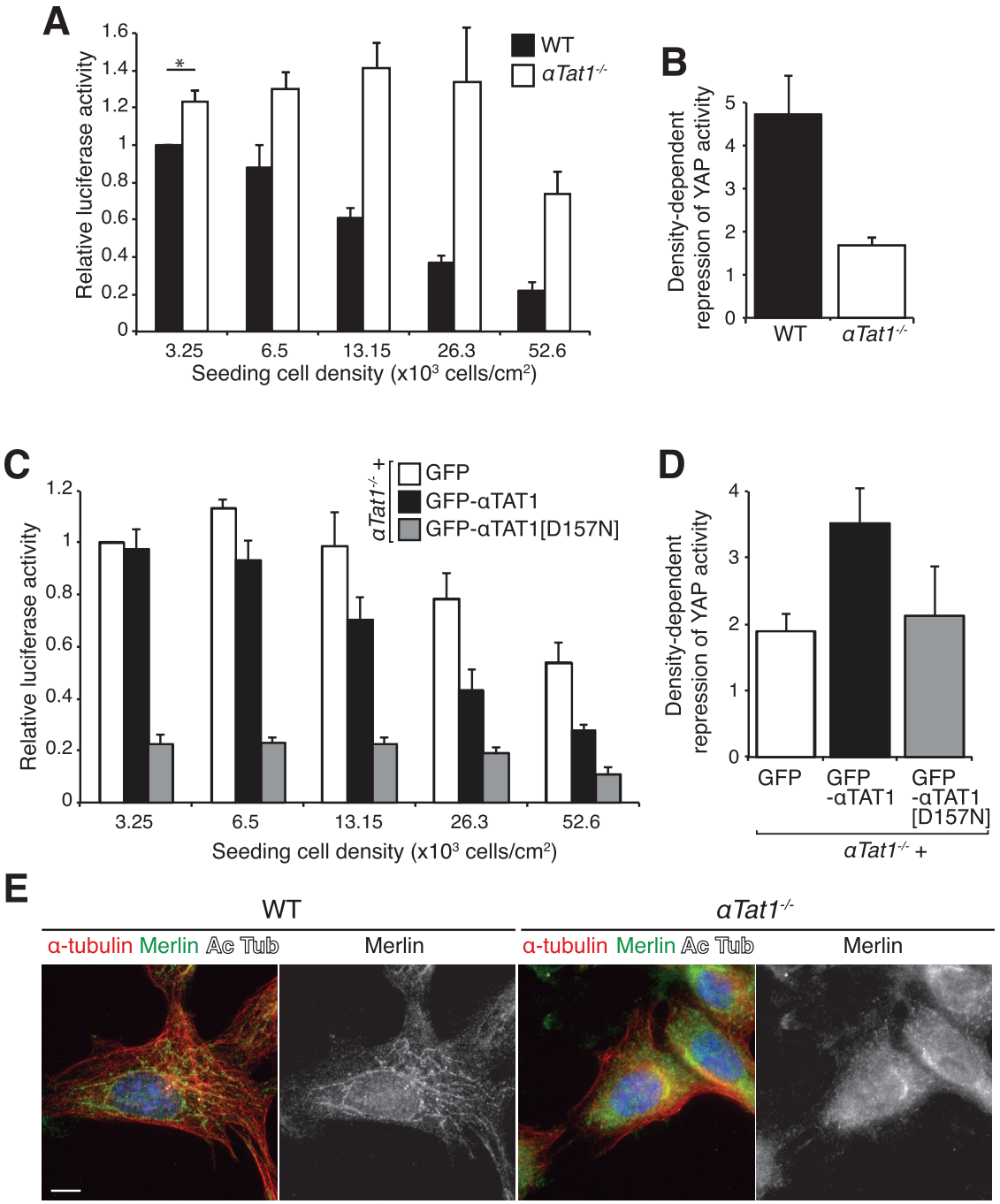

FIGURE 3: *αTat1* is essential for proper Hippo signaling (A) YAP/TAZ luciferase assay (8XGTIIC-luc) in wild-type (WT) and *αTat1*$^{-/-}$ cells seeded at increasing densities. Whereas YAP/TAZ activity is down-regulated with increasing cell density in WT cells, knockout cells exhibit a high luciferase signal even at the highest cell density. Relative luciferase activity was normalized to the value of WT cells at the sparsest density. (B) Ratio of the relative luciferase activity for the lowest over the highest cell density in WT and *αTat1*$^{-/-}$ cells. This ratio reflects the cell's ability to down-regulate YAP/TAZ activity upon increasing cell density. (C) YAP/TAZ luciferase assay (8XGTIIC-luc) in *αTat1*$^{-/-}$ cells stably expressing GFP, GFP-αTat1, and GFP-αTAT1[D157N], seeded at increasing densities. Only GFP-αTAT1[D157N] rescues the unusually high levels of YAP/TAZ activity in *αTat1*$^{-/-}$ cells. (D) Ratio of the relative luciferase activity for the lowest over the highest cell density in *αTat1*$^{-/-}$ cells stably expressing GFP, GFP-αTat1, and GFP-αTAT1[D157N]. Only GFP-αTat1 was able to rescue YAP/TAZ activity down-regulation upon cell density increase in *αTat1*$^{-/-}$ cells. (E) WT and *αTat1*$^{-/-}$ cells were immunolabeled for Merlin and K40 acetylated and total α-tubulin. Whereas in WT cells merlin was localized to particles along the microtubules, it exhibited diffuse localization in *αTat1*$^{-/-}$ cells. Scale bar, 10 μm.

decrease in YAP/TAZ transcriptional activity. Our results indicate that the enzymatic activity of αTat1 is required for restrained proliferation through down-regulation of Hippo signaling at confluency but is dispensable for monolayer formation. Several studies reported a function for αTat1 independently of its enzymatic activity, possibly through its binding to the microtubule lattice (Topalidou *et al.*, 2012;

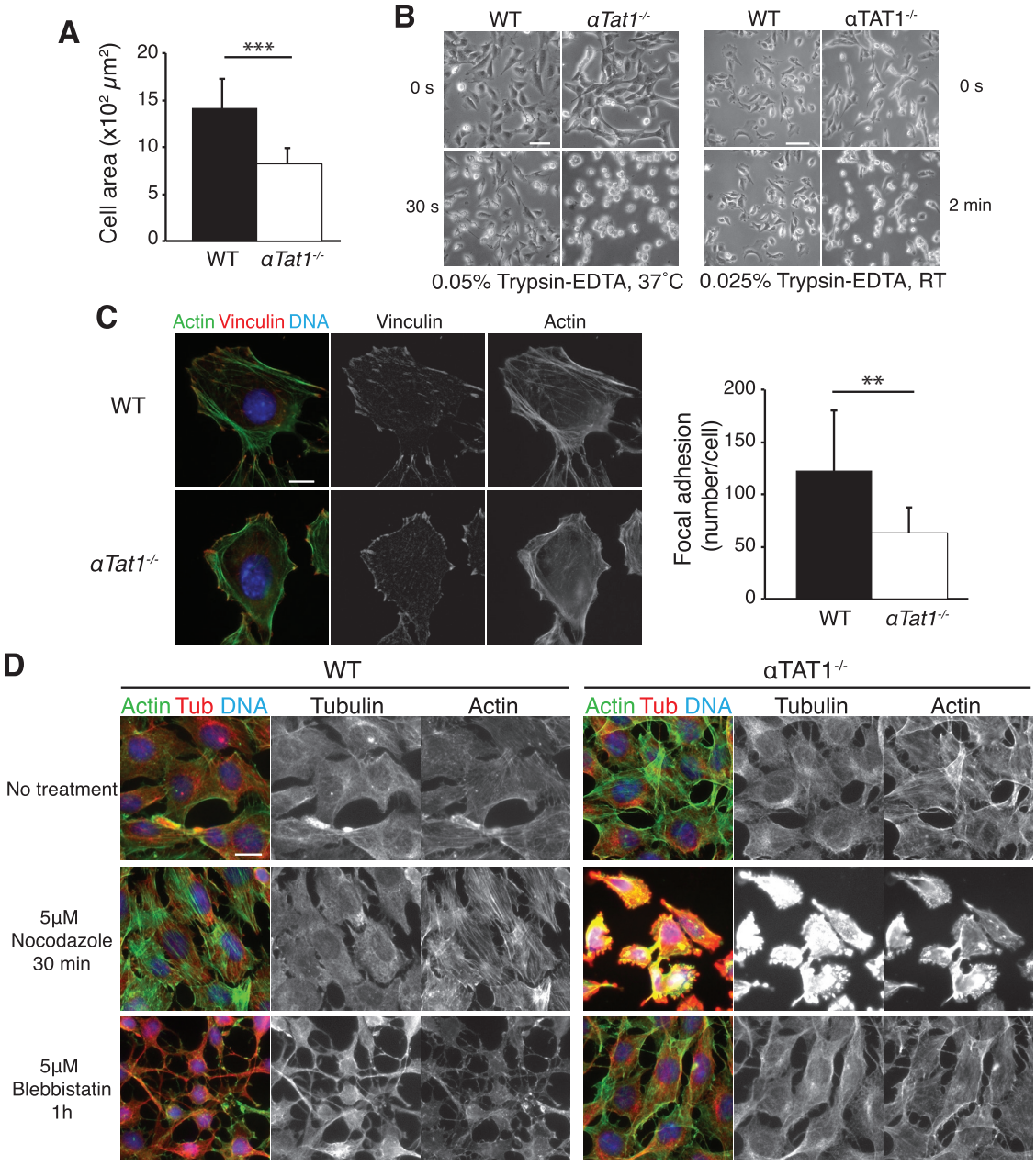

FIGURE 4: αTat1 is required for cell adhesion. (A) The surface area of $\alpha Tat1^{+/+}$ and $\alpha Tat1^{-/-}$ cells was measured using ImageJ ($n = 10$ cells/genotype). Knockout cells have a very significant decrease in cell area compared with wild-type cells ($p = 7.5 \times 10^{-5}$). (B) $\alpha Tat1^{+/+}$ and $\alpha Tat1^{-/-}$ cells were trypsinized with 37°C, 0.05% trypsin-EDTA or 0.025%, room temperature trypsin-EDTA. At the time points shown, trypsin-EDTA has little effect on wild-type cells, yet it rounds up most $\alpha Tat1^{-/-}$ cells. (C) $\alpha Tat1^{+/+}$ and $\alpha Tat1^{-/-}$ cells were labeled with an anti-vinculin antibody (red) and Alexa 488–phalloidin (green). The $\alpha Tat1^{-/-}$ cells showed reduced number of stress fibers and disorganized actin cytoskeleton. Using ImageJ, we quantified the number of focal adhesions per cell and found that it decreased in $\alpha Tat1^{-/-}$ cells compared with wild-type ($p = 0.01$, $n = 10$ cells/genotype). (D) $\alpha Tat1^{+/+}$ and $\alpha Tat1^{-/-}$ cells were treated with nocodazole or blebbistatin and immunostained for α-tubulin (red). Actin was labeled using Alexa 488–phalloidin (green). Whereas nocodazole treatment stimulates stress fiber formation in wild-type cells, no or few stress fibers were observed in $\alpha Tat1^{-/-}$ cells, which rounded up and detached. In blebbistatin-treated wild-type cells, the inhibition of myosin II function induces cytoplasmic collapse. In $\alpha Tat1^{-/-}$ cells, blebbistatin treatment did not yield any major morphological alteration. See Supplemental Figure S5 for a shorter exposure, where the fluorescence levels of $\alpha Tat1^{-/-}$ cells treated with nocodazole are not saturated. The apparent increase in tubulin and actin staining in $\alpha Tat1^{-/-}$ cells treated with nocodazole is likely due the rounding up of cells, which will generate a significant amount of out-of-focus fluorescence captured by epifluorescence. $^{**}p \leq 0.01$, $^{***}p \leq 0.001$, two-sided Wilcoxon test. Scale bars: B, 50 μm (left), 100 μm (right); C, 10 μm; D, 15 μm.

Kalebic *et al.*, 2013a; Howes *et al.*, 2014). Further, our results suggest that it is the pronounced dampening of YAP/TAZ activity in response to increasing cell density rather than the absolute activity of YAP/TAZ that is critical for contact inhibition of proliferation.

The striking loss of contact inhibition observed in *αTat1*$^{-/-}$ cells contrasts with the absence of any obvious defective proliferation in *αTat1*$^{-/-}$ mice. Here, we consider two hypotheses. First, this apparent discrepancy could stem from the different environment the cells experience in vivo and in vitro. In vitro, the lack of environmental factors that restrain cell proliferation inside tissues (low substrate stiffness, limited growth factor availability, high mechanical and spatial three-dimensional constraint, extracellular matrix abundance and diversity) creates a more permissive and stimulating environment for cell proliferation (Aragona *et al.*, 2013). These environmental conditions could therefore reveal a defective regulation of cell proliferation that is masked in vivo. Second, hyperproliferation caused by compromised contact inhibition could be contained by the strict mechanisms that regulate cell number at the tissular scale in vivo. Indeed, classic studies on compensatory proliferation showed that an increase in apoptotic cell number, sensed at the tissular level, triggers hyperproliferation, resulting in a tissue containing the correct cell number (Fan and Bergmann, 2008). Conversely, as illustrated by recent studies on overcrowding in epithelia (Eisenhoffer *et al.*, 2012; Marinari *et al.*, 2012), powerful homeostatic mechanisms maintain proper cell number by triggering cell extrusion and ultimately cell death. Therefore, in *αTat1*$^{-/-}$ mice, compensatory apoptosis at the tissue level could remove the supernumerary cells, resulting in normal-size organs in the adult.

We note that loss of microtubule acetylation does not appear to initiate carcinogenesis. However, this only indicates that loss of microtubule acetylation is not a driver for tumorigenesis. Therefore it remains conceivable that *αTat1*$^{-/-}$ mice may suffer from accelerated tumor development or generate more metastatic tumors when placed in a sensitized background for cancer emergence.

Reduction of focal adhesion number in *αTat1*-deficient cells

Genetic ablation of HDAC6 reduces microtubule dynamics and leads to decreased FA turnover, suggesting a role for tubulin acetylation in FA dynamics (Tran *et al.*, 2007). However, HDAC6 alters microtubule dynamics independently of its catalytic function toward tubulin (Zilberman *et al.*, 2009), making it unclear whether acetylated tubulin itself is involved in FA dynamics.

Cellular adhesive structures comprise small transient nascent FAs that easily detach when placed under tension and large mechanosensitive FAs that grow under tension of the actin stress fibers (Schiller *et al.*, 2013). Because *αTat1*-deficient cells display fewer and smaller FAs, an intriguing possibility is that acetylated microtubules bear mechanosensitive functions that help small FAs mature into large FAs. Alternatively, the presence of αTAT1 at FAs and the acetylation of cortactin by αTAT1 (Castro-Castro *et al.*, 2012) may suggest a more direct role of αTAT1 in FA dynamics.

Future analysis of FA mechanical properties should determine whether large mechanosensitive FAs are specifically affected in *αTat1*-deficient cells. Furthermore, evaluation of FA growth, maturation, and turnover will determine the mechanism by which αTat1 alters FAs. Finally, analysis of *αTat1*$^{-/-}$ MEFs stably expressing the catalytically dead form of αTat1 will clarify whether the acetyltransferase function of αTat1 modulates FA dynamics.

In this study, we show that Hippo signaling is defective in *αTat1*$^{-/-}$ MEFs even in individual cells that do not contact other cells (Figure 3A and Supplemental Figure S4C). Because the Hippo pathway and cell–substrate adhesion are closely linked (Lee *et al.*, 2001; Glantschnig *et al.*, 2002; Katagiri *et al.*, 2006; Artemenko *et al.*, 2012), it is tempting to consider that defective Hippo signaling and cell–substrate adhesion might share a common causality in *αTat1*-deficient cells. Here we consider two possibilities. First, αTat1 loss could affect the Hippo pathway through its effect on the actin cytoskeleton. Indeed, we show that αTat1 is required for proper FA number and actin cytoskeleton organization, and recent work found that a functional actin cytoskeleton is required for Hippo signaling (Dupont *et al.*, 2011; Wada *et al.*, 2011; Aragona *et al.*, 2013). Second, αTat1 loss could directly impair the Hippo pathway, which in turn is known to affect cell–substrate adhesion (Lee *et al.*, 2001; Glantschnig *et al.*, 2002; Katagiri *et al.*, 2006; Artemenko *et al.*, 2012). In support of the latter hypothesis, we show that αTat1 feeds rather directly into the Hippo pathway by controlling Merlin localization.

Gaining an understanding of oncogenic transformation through αTat1

Despite an absence of overt phenotype in the HDAC6-knockout mice (Zhang *et al.*, 2008), there is strong evidence for HDAC6 dysfunction participating in oncogenic transformation and tumor formation (Lee *et al.*, 2008). However, because HDAC6 deacetylates multiple substrates (Hubbert *et al.*, 2002; Bali *et al.*, 2005; Zhang *et al.*, 2007; Parmigiani *et al.*, 2008), it has been unclear whether the role of HDAC6 in oncogenic transformation is related to tubulin acetylation. Here we show that loss of αTat1, and in particular its catalytic activity, leads to reduced cell adhesion and loss of contact inhibition, two hallmarks of oncogenic transformation (Hanahan and Weinberg, 2011). Thus our results suggest a role for αTat1 in oncogenic transformation. Further work is required to assess whether *αTat1*-deficient cells have indeed acquired a carcinogenic potential by testing their anchorage-independent growth on soft agar and their tumorigenic potential when injected in mice. Understanding the precise involvement of acetylated microtubules in tumorigenesis and metastasis will be instrumental in defining therapeutic strategies based on the chemical manipulation of tubulin acetylation.

MATERIALS AND METHODS

Transgenic mice

All animal care and procedures were performed under a protocol approved by the Administrative Panel on Laboratory Animal Care at Stanford University (Stanford, CA). *Atat1*$^{tm1(KOMP)Vlcg}$ heterozygous ES cells were obtained from the KOMP repository (Davis, CA; www.komp.org). The ES cells were injected into C57BL6 blastocytes and implanted in receiving females at the Transgenic Research Center at Stanford University. We mated resulting chimeric males with albino C57BL6 females purchased from JAX (Sacramento, CA) to achieve germline transmission. Heterozygous males and females were then mated to obtain *αTAT1*$^{-/-}$ and *αTAT1*$^{+/+}$ mice.

Mice were genotyped by PCR of genomic DNA using the following primers: GGGCACAGACCTACAAAAGG (P1, common to both alleles), GTCAGACACTCGCTAGGTTACAG (P2, wild-type allele), and CTCCCCGTTCAAAGATCTGAG (P3, *αTAT1*$^{-/-}$ allele).

Cell culture and cell treatments

MEFs were derived from embryonic day (E) 14.5 *αTat1*$^{-/-}$ and *αTat1*$^{+/+}$ mice using standard procedures. Briefly, the head, heart, liver, and limbs were removed. The embryos were then enzymatically dissociated by incubation in a 0.05% trypsin-EDTA solution for 30 min at room temperature. After mechanical dissociation by pipetting, the cell suspension was plated in DMEM 15% fetal bovine serum (FBS), 0.05 mM β-mercaptoethanol, 1% L-glutamine, and

1% nonessential amino acids. The MEFs were then immortalized following a 3T3 protocol: attached surviving cells were split at 1:3 every 3 d for >30 passages. 3T3s were cultured in DMEM 10% FBS, 0.05 mM β-mercaptoethanol, 1% L-glutamine, and 1% nonessential amino acids.

For assessment of cellular adhesion strength to their substrate, cells were plated at 60,000 cells/ml on glass coverslips. After 24 h, cells were incubated either in a 37°C, 0.05% trypsin-EDTA solution for 30 s or in a room temperature, 0.025% trypsin-EDTA solution for 2 min.

To test the cross-talk between microtubules and the actin cytoskeleton, cells were plated at 70,000 cells/well (24-well plate) on 100 µg/ml fibronectin-coated glass coverslips and treated with 5 µM nocodazole for 30 min or 5 µM blebbistatin for 1 h in conditioned medium. After fixation (10 min in paraformaldehyde [PFA] 4% at room temperature), cells were processed for immunofluorescence.

To generate *αTat1*$^{-/-}$ cells stably expressing GFP, GFP-αTAT1, and GFP-αTAT1[D157N], we generated retroviruses using derivatives of pBabe-Puro (Shida *et al.*, 2010). Then *αTat1*-deficient cells were infected. After puromycin selection, single-cell clones were isolated and subjected to fluorescence-activated cell sorting (FACS) at the Stanford Shared FACS facility for moderate expression. The GFP-αTAT1 clone was chosen to match wild-type levels of acetylated α-tubulin by immunoblotting. GFP and GFP-αTAT1[D157N] clones were chosen to match GFP-αTAT1 expression levels.

Growth curve

To assess contact inhibition of proliferation, cells were plated at 15,000 cells/cm^2 in 35-mm culture dishes or on glass coverslips in 24-well plates. Medium was changed at days 1 and 3. Cells in the 35-mm culture dishes were trypsinized and counted with trypan blue every day on a hematocytometer. The cells plated on coverslips were fixed for 10 min in phosphate buffered saline (PBS)–4% PFA at days 1 and 5 and processed for immunofluorescence.

Antibodies and reagents

The following primary antibodies were used: rabbit anti-αTat1 (homemade antibody purified according to standard protocols), mouse anti–α-tubulin (12G10; Developmental Studies Hybridoma Bank, Iowa City, IA), mouse anti–K40 acetylated α-tubulin (mouse, 611B; Sigma-Aldrich, St. Louis, MO), rabbit anti–detyrosinated α-tubulin (gift from Gregg Gundersen, Columbia University, New York, NY), mouse anti–glutamylated α-tubulin (GT335; gift from Carsten Janke, Institut Curie, Orsay, France), rat anti–tyrosinated α-tubulin (clone YL1/2; Chemicon, Billerica, MA), rabbit anti–polyglutamylated α-tubulin (polyE, serum; gift from Carsten Janke), rabbit anti-GFP (homemade; Nachury *et al.*, 2007), rabbit anti-S100β (Sigma-Aldrich), rabbit anti-GFAP (Dako, Carpinteria, CA), mouse anti-vinculin (clone hVIN-1; Sigma-Aldrich), rabbit anti-ZO1 (Invitrogen, Grand Island, NY), mouse anti–α-tubulin (clone DM1A; Thermo Scientific, Waltham, MA), rabbit anti-Arl13B (Proteintech, Chicago, IL), rabbit anti-GFP (A11122; Invitrogen), and rabbit anti-Merlin/NF2 (A19, sc-331; Santa Cruz Biotechnology, Dallas, TX).

For immunoblotting, primary antibodies were used at the following dilutions: anti-αTat1 (1 µg/ml), anti–α-tubulin (12G10, 1/5000; DM1A, 1/500), anti–K40 acetylated α-tubulin (1/6000), anti–detyrosinated α-tubulin (1/50,000), anti–glutamylated α-tubulin (1/1000), anti–tyrosinated α-tubulin (1/100), anti–polyglutamylated α-tubulin (1/4000), and anti-GFP (1/1000).

For immunofluorescence, primary antibodies were diluted as indicated: anti–K40 acetylated α-tubulin (1/500), anti–detyrosinated α-tubulin (1/800), anti–tyrosinated α-tubulin (1/100), anti-S110β (1/100), anti-GFAP (1/500), anti–glutamylated α-tubulin (1/1000), anti-vinculin (1/800), anti-ZO1 (1/400), anti-Arl13B (1/800), anti–α-tubulin (DM1A, 1/1000), and anti-Merlin/NF2 (1/25).

Immunoblots were developed with fluorescent secondary antibodies (DyLight 800 goat anti-mouse, anti-rat, anti-rabbit, 1:15,000; Thermo) and visualized by infrared laser scanner (Odyssey, Licor, Lincoln, NE; Figures 1 and 2) or with horseradish peroxidase–conjugated protein A (1/10,000 Invitrogen) or anti-mouse antibody (1/15,000; Jackson ImmunoResearch, West Grove, PA) and enhanced chemiluminescence (Figure 4 and Supplemental Figures S1 and S3).

Alexa Fluor–conjugated secondary antibodies (1/2000; Molecular Probes, Eugene, OR) were used for immunofluorescence. Actin was labeled with Alexa Fluor 488–phalloidin (1/40 in 1% PBS–bovine serum albumin; Molecular Probes) for 20 min after secondary antibodies. Finally, nuclei were stained with Hoechst (1/10,000).

Immunoblotting

Mice were killed by isoflurane overdose and cervical dislocation. Brains were sonicated and lysed in a buffer containing 137 mM NaCl, 20 mM Tris, pH 7.5, 1% Triton X, 10% glycerol, and protease inhibitors (1 ml of buffer/100 mg of brain). Cells were scraped and lysed in RIPB buffer (25 mM Tris-HCl, pH 7.5, 300 mM NaCl, 1 mM EGTA, 0.5% Triton X-100). Lysates were run on a NuPAGE 4–12% Bis-Tris gel, and membranes were blotted following standard procedures. For the αTat1 and α-tubulin immunoblots (Figure 1A), 20 µg of total protein was run in each lane for all stages except E14.5 (5 µg). For the other PTMs, 200 ng (detyrosinated, PolyE, acetylated, tyrosinated, and total α-tubulin) and 2 µg (polyglutamylated GT335 α-tubulin) were run (Figure 1D). Immunoblots on cell lysates were done by loading 10 µg (acetylated α-tubulin) and 3 or 5 µg (total α-tubulin) of protein. All fluorescence signals were quantitated with the Odyssey imaging system and were within the linear range of the instrument.

Immunofluorescence and histological staining

Immunohistochemistry and histological staining. Brains were fixed by intracardiac perfusion of 4% PFA in PBS, washed overnight in PBS, and cryoprotected in PBS–30% sucrose for 24 h. Cryosections, 12 µm, were cut and air-dried. For the analysis of brain morphology, sections were stained with Mayer's hematoxylin and Eosin Y solutions (Electron Microscopy Science, Hatfield, PA) using standard protocols. For immunostaining, the sections were incubated in blocking buffer (10% FBS, 0.1% Triton X-100 in PBS) for 1 h and then in primary antibodies diluted in blocking solution for 1 h or overnight. After washing, sections were incubated in Alexa Fluor–conjugated corresponding secondary antibodies in blocking buffer for 1 h.

For corneal endothelium whole-mount immunostaining, mice were killed by overdose of isoflurane (Baxter, Deerfield, IL) and cervical dislocation or perfused as described before. Eyes were extracted and fixed or postfixed (if perfused) by immersion in 4% PFA in PBS for 20 min. The corneas were then dissected out, washed, and incubated in blocking buffer for 30 min and in primary antibodies for 1 h. Nuclei were stained with Hoechst.

Immunocytochemistry. Cells were seeded either at 70,000 cells/well on 100 µg/ml fibronectin (Figure 3D) or on glass (Supplemental Figure S4C) or at 30,000 cells/well (Figure 3C) on 20 µg/ml fibronectin. After 24 h, cells were fixed in PBS–4% PFA for 10 min at room temperature (or for 10 min in methanol at –20°C for Merlin immunofluorescence) and processed for immunofluorescence. For

ELP3 expression in $\alpha TAT1^{-/-}$ cells, 20,000 cells/well were seeded on glass. After 24 h of culture, cells were transfected with GFP-ELP3 (gift from L. Nguyen, Liege University, Wallonia, Belgium) and X-tremeGENE 9 (Roche, Indianapolis, IN) and fixed the next day.

For immunofluorescence, the cells were blocked for 30 min and incubated in primary antibody in blocking solution for 1 h, in secondary for 30 min, and in Alexa Fluor 488–phalloidin for 20 min.

Imaging

Histologically stained brain sections were imaged on an Olympus stitching microscope. Images of immunolabeled brain sections and MEFs were acquired on an Everest workstation (Intelligent Imaging Innovations, Denver, CO) built around an AxioImager M1 (Zeiss, Thornwood, NY) fitted with a CoolSNAP HQ2 CCD camera (Photometrics, Tucson, AZ). The objectives used were a PlanApo 63×/1.4, PlanNeoFluar 40×/0.75, and PlanNeoFluar 10×/0.3 (Olympus, Central Valley, PA). For FA number quantification, cells were imaged on a DeltaVision system (Applied Precision, Issaquah, WA) equipped with a PlanApo 60×/1.40 objective lens and a Scientific CMOS camera.

The cells subjected to trypsin were imaged on a Leica DM IL inverted microscope with a 20× objective Leica Highplan 1 20×/0.3

Luciferase assay

Wild-type, $\alpha Tat1^{-/-}$, and $\alpha Tat1^{-/-}$ stably expressing GFP, GFP-αTAT1, and GFP-αTAT1[D157N] MEFs were seeded at the indicated densities on plastic in 24-well plates. The next day, the cells were cotransfected with the YAP reporter 8xGTIIC-lux (plasmid 34615, 100 ng/well; Addgene, Cambridge, MA), pRL-SV40 (20 ng/well; Promega, Madison, WI), and pEF5B-FRT-GFP-GFP-FKBP (680 ng/well, to keep DNA content constant across samples), using 2 µl of Lipofectamine 2000 (Life Technologies). Samples were harvested 24 h after transfection and assayed for *Renilla* and firefly luciferase using homemade luciferase buffer in a Modulus Microplate Multimode Reader (Turner Biosystems, Promega).

Cell area and focal adhesion quantification

Cell area was manually measured using the polygon selection tool of ImageJ (National Institutes of Health, Bethesda, MD). For focal adhesion number quantification, pictures were deconvolved using SoftWoRx 6.0 (Applied Precision, three-dimensional iterative constrained deconvolution, enhanced ratio, 10 iterations), submitted to the rolling ball background subtraction on ImageJ (rolling ball radius of 20 pixels), and the threshold adjusted so that only FAs are selected in wild-type cells. Objects >0.03 pixel (the size of the smaller FA adhesion) were counted with the command Analyze Particles.

Measurement of cell size

Cells were seeded at 720,000 cells per well in a six-well plate, grown for 2 d, and trypsinized. Cell size was determined by measuring the forward scatter (FSC-A) by flow cytometry with a BD Accuri C6.

Audiology tests

Adult mice were anesthetized admitting 100 mg/kg ketamine and 15 mg/kg xylazine intraperitoneally, and their body temperature was maintained at 37°C until fully recovered.

Sound stimuli were generated digitally by a Matlab 2010b–controlled (MathWorks, Torrance, CA), custom-built acoustic system using a digital-to-analogue converter (BNC-2090A; National Instruments) sampling at 200 kHz, a sound amplifier, and two high-frequency speakers (Pyramid TW125). The speakers were connected to an ear bar and calibrated in the ear canal before each experiment using a probe-tip microphone (microphone type 4182, NEXUS conditioning amplifier; Brüel and Kjaer, Denmark).

Auditory brainstem response. Auditory brainstem response (ABR) was recorded by placing three needle electrodes subcutaneously at the vertex, below the left ear, and a ground electrode close to the tail. The signals were amplified 10,000 times using a biological amplifier (DP-311; Warner Instruments, Hamden, CT) digitized at 200 kHz (BNC-2090A; National Instruments, Austin, TX) and digital band-pass filtered from 300 to 3000 Hz. The stimulus for eliciting the ABR was a 5-ms sine wave tone pip with cos2 envelope rise and fall times of 0.5 ms. Repetition time was 50 ms, and 260 trials were averaged.

At each frequency, the peak ABR at stimulus intensities ranging from 10 to 80 dB sound pressure levels was measured in 10-dB steps and interpolated to find threshold five SDs above the noise floor.

Distortion products of otoacoustic emission. For stimulation of distortion products of otoacoustic emissions (DPOAEs), two sine wave tones of equal intensity (l1 = l2) and 1-s duration were presented to the ear. The two tones ranged from 20 to 80 dB SPL attenuated in 10-dB increments, and the two frequencies (f2 = 1.2f1) ranged from f2 with 4–46 kHz. The acoustic signal was detected by a microphone in the ear bar and was sampled at 200 kHz (BNC-2090A; National Instruments), and the magnitude of the cubic distortion product (2f1 − f2) was determined by fast Fourier transform. The surrounding noise floor was also calculated by averaging 20 adjacent frequency bins around the distortion product frequency. DPOAE thresholds were reached when the signal was >2 SDs above the noise floor.

Statistical analysis

The results are presented as mean ± SD. Statistical significance was determined using a two-sided Wilcoxon test.

ACKNOWLEDGMENTS

We thank T. Südhof (Stanford University) for generously sharing microscopes; G. R. Crabtree for generously sharing the Microplate Reader; S. Dong and K. C. Garcia (Stanford University) for the flow cytometry experiment; P. Beachy and M. Monje-Diesseroth (Stanford University), G. Gundersen, C. Janke, L. Nguyen, and S. Piccolo (University of Padova, Padova, Italy) for sharing antibodies and plasmids; and members of the Nachury lab for stimulating discussions. The 12G10 antibody was developed under the auspices of the National Institute of Child Health and Human Development and was provided by the Developmental Studies Hybridoma Bank (University of Iowa, Iowa City, IA). This work was supported by grants from the National Institutes of Health (GM089933 to M.V.N., DC010363 to S.H., and EY022639 to C.I. and the Human Frontier Science Foundation (RGY0088/2012 to M.V.N.).

REFERENCES

Abercrombie M (1962). Contact-dependent behavior of normal cells and the possible significance of surface changes in virus-induced transformation. Cold Spring Harb Symp Quant Biol 27, 427–431.

Abercrombie M (1979). Contact inhibition and malignancy. Nature 281, 259–262.

Akella JS, Wloga D, Kim J, Starostina NG, Lyons-Abbott S, Morrissette NS, Dougan ST, Kipreos ET, Gaertig J (2010). MEC-17 is an alpha-tubulin acetyltransferase. Nature 467, 218–222.

Aragona M, Panciera T, Manfrin A, Giulitti S, Michielin F, Elvassore N, Dupont S, Piccolo S (2013). A mechanical checkpoint controls multicellular growth through YAP/TAZ regulation by actin-processing factors. Cell 154, 1047–1059.

Artemenko Y, Batsios P, Borleis J, Gagnon Z, Lee J, Rohlfs M, Sanseau D, Willard SS, Schleicher M, Devreotes PN (2012). Tumor suppressor Hippo/MST1 kinase mediates chemotaxis by regulating spreading and adhesion. Proc Natl Acad Sci USA 109, 13632–13637.

Bali P *et al.* (2005). Inhibition of histone deacetylase 6 acetylates and disrupts the chaperone function of heat shock protein 90: a novel basis for antileukemia activity of histone deacetylase inhibitors. J Biol Chem 280, 26729–26734.

Bensenor LB, Barlan K, Rice SE, Fehon RG, Gelfand VI (2010). Microtubule-mediated transport of the tumor-suppressor protein Merlin and its mutants. Proc Natl Acad Sci USA 107, 7311–7316.

Berndsen CE, Denu JM (2008). Catalysis and substrate selection by histone/protein lysine acetyltransferases. Curr Opin Struct Biol 18, 682–689.

Bershadsky A, Chausovsky A, Becker E, Lyubimova A, Geiger B (1996). Involvement of microtubules in the control of adhesion-dependent signal transduction. Curr Biol 6, 1279–1289.

Blitzer AL, Panagis L, Gusella GL, Danias J, Mlodzik M, Iomini C (2011). Primary cilia dynamics instruct tissue patterning and repair of corneal endothelium. Proc Natl Acad Sci USA 108, 2819–2824.

Cai D, McEwen DP, Martens JR, Meyhofer E, Verhey KJ (2009). Single molecule imaging reveals differences in microtubule track selection between kinesin motors. PLoS Biol 7, e1000216.

Castro-Castro A, Janke C, Montagnac G, Paul-Gilloteaux P, Chavrier P (2012). ATAT1/MEC-17 acetyltransferase and HDAC6 deacetylase control a balance of acetylation of alpha-tubulin and cortactin and regulate MT1-MMP trafficking and breast tumor cell invasion. Eur J Cell Biol 91, 950–960.

Cheishvili D, Maayan C, Cohen-Kupiec R, Lefler S, Weil M, Ast G, Razin A (2011). IKAP/Elp1 involvement in cytoskeleton regulation and implication for familial dysautonomia. Hum Mol Genet 20, 1585–1594.

Creppe C *et al.* (2009). Elongator controls the migration and differentiation of cortical neurons through acetylation of alpha-tubulin. Cell 136, 551–564.

Cueva JG, Hsin J, Huang Kerwyn C, Goodman, Miriam B (2012). Post-translational acetylation of α-tubulin constrains protofilament number in native microtubules. Curr Biol 22, 1066–1074.

Dompierre JP, Godin JD, Charrin BC, Cordelieres FP, King SJ, Humbert S, Saudou F (2007). Histone deacetylase 6 inhibition compensates for the transport deficit in Huntington's disease by increasing tubulin acetylation. J Neurosci Methods 27, 3571–3583.

Dupont S *et al.* (2011). Role of YAP/TAZ in mechanotransduction. Nature 474, 179–183.

Eisenhoffer GT, Loftus PD, Yoshigi M, Otsuna H, Chien CB, Morcos PA, Rosenblatt J (2012). Crowding induces live cell extrusion to maintain homeostatic cell numbers in epithelia. Nature 484, 546–549.

Fan Y, Bergmann A (2008). Apoptosis-induced compensatory proliferation. The cell is dead. Long live the cell!. Trends Cell Biol 18, 467–473.

Friedmann DR, Aguilar A, Fan J, Nachury MV, Marmorstein R (2012). Structure of the alpha-tubulin acetyltransferase, alphaTAT1, and implications for tubulin-specific acetylation. Proc Natl Acad Sci USA 109, 19655–19660.

Gilmer S, Clay P, MacRae TH, Fowke LC (1999). Acetylated tubulin is found in all microtubule arrays of two species of pine. Protoplasma 207, 174–185.

Glantschnig H, Rodan GA, Reszka AA (2002). Mapping of MST1 kinase sites of phosphorylation. Activation and autophosphorylation. J Biol Chem 277, 42987–42996.

Hanahan D, Weinberg RA (2000). The hallmarks of cancer. Cell 100, 57–70.

Hanahan D, Weinberg RA (2011). Hallmarks of cancer: the next generation. Cell 144, 646–674.

Howes SC, Alushin GM, Shida T, Nachury MV, Nogales E (2014). Effects of tubulin acetylation and tubulin acetyltransferase binding on microtubule structure. Mol Biol Cell 25, 257–266.

Huang RF, Lloyd CW (1999). Gibberellic acid stabilises microtubules in maize suspension cells to cold and stimulates acetylation of alpha-tubulin. FEBS Lett 443, 317–320.

Hubbert C, Guardiola A, Shao R, Kawaguchi Y, Ito A, Nixon A, Yoshida M, Wang XF, Yao TP (2002). HDAC6 is a microtubule-associated deacetylase. Nature 417, 455–458.

Janke C, Bulinski JC (2011). Post-translational regulation of the microtubule cytoskeleton: mechanisms and functions. Nat Rev Mol Cell Biol 12, 773–786.

Kalebic N, Martinez C, Perlas E, Hublitz P, Bilbao-Cortes D, Fiedorczuk K, Andolfo A, Heppenstall PA (2013a). Tubulin acetyltransferase alphaTAT1 destabilizes microtubules independently of its acetylation activity. Mol Cell Biol 33, 1114–1123.

Kalebic N, Sorrentino S, Perlas E, Bolasco G, Martinez C, Heppenstall PA (2013b). alphaTAT1 is the major alpha-tubulin acetyltransferase in mice. Nat Commun 4, 1962.

Katagiri K, Imamura M, Kinashi T (2006). Spatiotemporal regulation of the kinase Mst1 by binding protein RAPL is critical for lymphocyte polarity and adhesion. Nat Immunol 7, 919–928.

Kim GW, Li L, Gorbani M, You L, Yang XJ (2013). Mice lacking alpha-tubulin acetyltransferase 1 are viable but display alpha-tubulin acetylation deficiency and dentate gyrus distortion. J Biol Chem 288, 20334–20350.

Lee KK, Ohyama T, Yajima N, Tsubuki S, Yonehara S (2001). MST, a physiological caspase substrate, highly sensitizes apoptosis both upstream and downstream of caspase activation. J Biol Chem 276, 19276–19285.

Lee YS, Lim KH, Guo X, Kawaguchi Y, Gao Y, Barrientos T, Ordentlich P, Wang XF, Counter CM, Yao TP (2008). The cytoplasmic deacetylase HDAC6 is required for efficient oncogenic tumorigenesis. Cancer Res 68, 7561–7569.

Li L, Wei D, Wang Q, Pan J, Liu R, Zhang X, Bao L (2012). MEC-17 deficiency leads to reduced alpha-tubulin acetylation and impaired migration of cortical neurons. J Neurosci 32, 12673–12683.

Marinari E, Mehonic A, Curran S, Gale J, Duke T, Baum B (2012). Live-cell delamination counterbalances epithelial growth to limit tissue overcrowding. Nature 484, 542–545.

McClatchey AI, Yap AS (2012). Contact inhibition (of proliferation) redux. Curr Opin Cell Biol 24, 685–694.

Miskiewicz K *et al.* (2011). ELP3 controls active zone morphology by acetylating the ELKS family member bruchpilot. Neuron 72, 776–788.

Muranen T, Gronholm M, Lampin A, Lallemand D, Zhao F, Giovannini M, Carpen O (2007). The tumor suppressor merlin interacts with microtubules and modulates Schwann cell microtubule cytoskeleton. Hum Mol Genet 16, 1742–1751.

Nachury MV *et al.* (2007). A core complex of BBS proteins cooperates with the GTPase Rab8 to promote ciliary membrane biogenesis. Cell 129, 1201–1213.

Nakagawa U, Suzuki D, Ishikawa M, Sato H, Kamemura K, Imamura A (2013). Acetylation of alpha-tubulin on Lys is a widespread post-translational modification in angiosperms. Biosci Biotechnol Biochem 77, 1602–1605.

North BJ, Marshall BL, Borra MT, Denu JM, Verdin E (2003). The human Sir2 ortholog, SIRT2, is an NAD+-dependent tubulin deacetylase. Mol Cell 11, 437–444.

Ohkawa N, Fujitani K, Tokunaga E, Furuya S, Inokuchi K (2007). The microtubule destabilizer stathmin mediates the development of dendritic arbors in neuronal cells. J Cell Sci 120, 1447–1456.

Ohkawa N, Sugisaki S, Tokunaga E, Fujitani K, Hayasaka T, Setou M, Inokuchi K (2008). N-acetyltransferase ARD1-NAT1 regulates neuronal dendritic development. Genes Cells 13, 1171–1183.

Palazzo A, Ackerman B, Gundersen GG (2003). Cell biology: tubulin acetylation and cell motility. Nature 421, 230.

Parmigiani RB, Xu WS, Venta-Perez G, Erdjument-Bromage H, Yaneva M, Tempst P, Marks PA (2008). HDAC6 is a specific deacetylase of peroxiredoxins and is involved in redox regulation. Proc Natl Acad Sci USA 105, 9633–9638.

Rosenbaum J (2000). Cytoskeleton: functions for tubulin modifications at last. Curr Biol 10, R801–R803.

Schiller HB *et al.* (2013). β1- and αv-class integrins cooperate to regulate myosin II during rigidity sensing of fibronectin-based microenvironments. Nat Cell Biol 15, 625–636.

Shida T, Cueva JG, Xu Z, Goodman MB, Nachury MV (2010). The major alpha-tubulin K40 acetyltransferase TAT1 promotes rapid ciliogenesis and efficient mechanosensation. Proc Natl Acad Sci USA 107, 21517–21522.

Shutova MS, Alexandrova AY, Vasiliev JM (2008). Regulation of polarity in cells devoid of actin bundle system after treatment with inhibitors of myosin II activity. Cell Motil Cytoskeleton 65, 734–746.

Smole Z, Thoma CR, Applegate KT, Duda M, Gutbrodt KL, Danuser G, Krek W (2014). Tumor suppressor NF2/merlin is a microtubule stabilizer. Cancer Res 74, 353–362.

Solinger JA, Paolinelli R, Kloss H, Scorza FB, Marchesi S, Sauder U, Mitsushima D, Capuani F, Sturzenbaum SR, Cassata G (2010). The *Caenorhabditis elegans* elongator complex regulates neuronal alpha-tubulin acetylation. PLoS Genet 6, e1000820.

Stehbens S, Wittmann T (2012). Targeting and transport: how microtubules control focal adhesion dynamics. J Cell Biol 198, 481–489.

Szarama KB, Gavara N, Petralia RS, Kelley MW, Chadwick RS (2012). Cytoskeletal changes in actin and microtubules underlie the developing surface mechanical properties of sensory and supporting cells in the mouse cochlea. Development 139, 2187–2197.
Tannenbaum J, Slepecky NB (1997). Localization of microtubules containing posttranslationally modified tubulin in cochlear epithelial cells during development. Cell Motil Cytoskeleton 38, 146–162.
Todaro GJ, Green H (1963). Quantitative studies of the growth of mouse embryo cells in culture and their development into established lines. J Cell Biol 17, 299–313.
Todaro GJ, Lazar GK, Green H (1965). The initiation of cell division in a contact-inhibited mammalian cell line. J Cell Physiol 66, 325–333.
Topalidou I *et al*. (2012). Genetically separable functions of the MEC-17 tubulin acetyltransferase affect microtubule organization. Curr Biol 22, 1057–1065 .
Tran AD *et al*. (2007). HDAC6 deacetylation of tubulin modulates dynamics of cellular adhesions. J Cell Sci 120, 1469–1479.
Wada K, Itoga K, Okano T, Yonemura S, Sasaki H (2011). Hippo pathway regulation by cell morphology and stress fibers. Development 138, 3907–3914.
Walter WJ, Beranek V, Fischermeier E, Diez S (2012). Tubulin acetylation alone does not affect kinesin-1 velocity and run length in vitro. PLoS One 7, e42218.
Wang N, Naruse K, Stamenovic D, Fredberg JJ, Mijailovich SM, Tolic-Norrelykke IM, Polte T, Mannix R, Ingber DE (2001). Mechanical behavior in living cells consistent with the tensegrity model. Proc Natl Acad Sci USA 98, 7765–7770.
Witte H, Neukirchen D, Bradke F (2008). Microtubule stabilization specifies initial neuronal polarization. J Cell Biol 180, 619–632.
Zeng Q, Hong W (2008). The emerging role of the hippo pathway in cell contact inhibition, organ size control, and cancer development in mammals. Cancer Cell 13, 188–192.
Zhang X *et al*. (2007). HDAC6 modulates cell motility by altering the acetylation level of cortactin. Mol Cell 27, 197–213.
Zhang Y *et al*. (2008). Mice lacking histone deacetylase 6 have hyperacetylated tubulin but are viable and develop normally. Mol Cell Biol 28, 1688–1701.
Zhao B, Li L, Wang L, Wang CY, Yu J, Guan KL (2012). Cell detachment activates the Hippo pathway via cytoskeleton reorganization to induce anoikis. Genes Dev 26, 54–68.
Zhao B, Tumaneng K, Guan KL (2011). The Hippo pathway in organ size control, tissue regeneration and stem cell self-renewal. Nat Cell Biol 13, 877–883.
Zilberman Y, Ballestrem C, Carramusa L, Mazitschek R, Khochbin S, Bershadsky A (2009). Regulation of microtubule dynamics by inhibition of the tubulin deacetylase HDAC6. J Cell Sci 122, 3531–3541.